

X-Ray Fluorescence Spectrometry in Art and Archaeology

Michael Mantler^{1*} and Manfred Schreiner²

¹ Institute of Applied and Technical Physics, Vienna University of Technology, Wiedner Hauptstrasse 8–10, A-1040 Vienna, Austria

² Institute of Chemistry, Academy of Fine Arts, Schillerplatz 3, A-1010 Vienna, Austria

This paper presents examples of analyses by x-ray fluorescence (XRF) spectrometry in art and archaeology, including pigments in paint layers and illuminated manuscripts, of iridescent glasses and of medieval coins. Theoretical aspects of information depths and shielding effects in layered materials are discussed. Element maps were experimentally obtained by a specially designed x-ray spectrometer (1 × 1 mm pixel resolution) and by electron-excited XRF (electron microprobe). Copyright © 2000 John Wiley & Sons, Ltd.

INTRODUCTION

Art historians, archaeologists and conservators are constantly concerned with the questions of where, when and by whom an object was made. Stylistic considerations combined with aesthetic evaluations and comprehensive archive studies can usually provide answers. However, styles were sometimes copied at locations and times completely different from those of their origin, and then investigations of the physical properties and chemical composition of the artifacts are helpful and increasingly applied to allocate an object to a particular historic or prehistoric context, to determine the correctness of the claimed provenance or to explore the technology used for the manufacturing. For example, the deliberate alloying of Cu with Sn, As, Sb and Pb has varied greatly from region to region and from time to time and careful material analysis combined with such knowledge can be used to presume the geographic origin of an object or at least the origin of the materials of which it was made.

Material analysis of our cultural heritage is almost as old as the scientific documentation of objects of art and archaeology. It was Martin H. Klaproth (1743–1817), Professor at the University in Berlin, who reported in 1795 the chemical composition of Roman coins, ancient alloys and glass^{1–4} based upon gravimetric analyses and newly developed chemical recipes for the separation of Cu, Pb and Sn, and their quantitative determination. For his studies large amounts of sample material, even whole small coins, had to be dissolved in nitric acid, a procedure which would nowadays not be accepted by the curators or conservators.

At the beginning of the 20th century, microchemical techniques^{5–11} and spot tests were developed,^{12,13} which significantly reduced the amount of sample material necessary for the analysis. A specific advantage of the classical microchemical analytical tests is that they provide

information on both inorganic and organic constituents. The greatest disadvantage of requiring a separate sample for each identification could be overcome by using several separation techniques.¹³ Therefore, it is not surprising that a number of museum laboratories and scientific laboratories specializing in the investigation of materials and techniques used for works of art were established in the first decades of the 20th century.

The booming development of electronics in recent decades has brought new analytical instruments, which have opened new horizons with respect to the origin or authenticity, technical conception and preservation of works of art.^{14–16} Among the most commonly cited analytical methods in the literature dealing with the investigation of inorganic materials such as pigments, glasses, ceramics, and metals are optical emission spectrometry (OES),^{11,17,18} atomic absorption spectrometry (AAS)^{17,19} and x-ray fluorescence (XRF) and x-ray diffractometry (XRD). For XRF all excitation methods are used including photons from x-ray tubes^{20,21} and synchrotrons, electrons [electron probe microanalysis (EPMA), scanning electron microscopy with energy-dispersive x-ray micro-analysis (SEM–EDX)]^{22,23} and protons [particle-induced x-ray emission (PIXE), particle-induced γ -ray emission (PIGE)].^{24–27} Additionally, neutron activation analysis (NAA) has provided a large number of data for archaeologists interested not only in the chemical composition of objects but also in the geographical and temporal origin of various materials. Studying the ratio of specific isotopes (e.g. $^{206}\text{Pb}/^{204}\text{Pb}$ or $^{16}\text{O}/^{18}\text{O}$) by mass spectrometry (MS) has, for example, enabled art historians to assign marbles to certain antique quarries.^{28,29}

THE ROLE OF XRF

XRF is a method for the qualitative and quantitative analysis of chemical elements. It is in principle applicable to all elements except the first two (H and He) of the periodic system, thereby covering an energy region from about 50 eV to 100 keV. However, many light elements

* Correspondence to: M. Mantler, Institute of Applied and Technical Physics, Vienna University of Technology, Wiedner Haupstrasse 8–10, A-1040 Vienna, Austria.

are difficult to measure and require advanced instrumentation, which often limits practical work to atomic numbers above 13 (A1). On the other hand, owing to costs of equipment and increasingly difficult radiation protection measures at high photon energies, L-lines rather than K-lines are measured at higher atomic numbers (above 50, Sn), so that the measured fluorescent photon energies are generally between 1 and 25 keV and excitation (tube) voltages less than 60 kV. The energy range is not only an analytical characteristic, but also important to estimate the danger of possible radiation damage. Another aspect is radiation protection for personnel involved in field analyses or when using specialized equipment with open beams in laboratories.

Neither the observed photon energies of fluorescent lines nor their intensities are noticeably affected by the chemical state of the analyzed atoms (except for very long wavelengths and very light elements) so that no destructive dissolution and/or atomization by a flame, arc, spark or plasma is required, as is generally the case in optical emission (and absorption) methods. In fact, not much specimen preparation is required at all, unless highly accurate quantitative analyses or homogenization is required. Homogenization may become an issue as many objects of art and archaeology are rather inhomogeneous by nature, and the question may arise of the extent to which the results from a limited analyzed volume represents the whole artifact. Such considerations are particularly important when corrosion layers, coatings or painted artifacts are analyzed, or when such layers absorb the radiation of an underlying analyzed material.

Rarely ever does the analysis of one or even a few elements answer all questions. Often the analyzed element is hoped to represent a pigment or an impurity related to the origin or to provide some other indirect hint. The phase of interest is often an oxide within a matrix of other oxides including the same analyzed element(s), sometimes embedded in organic binders as in the case of paints, and an unambiguous identification and exact quantification of the material of interest is impossible without employing complementary analytical methods.

Instrumentation plays an important role. Electron-excited XRF requires a small sample that sustains vacuum and has an electrically conductive surface; the method is ideally suited to analyze, for example, cross-sections of paints or element distributions at surfaces. Total reflection XRF is an ultimate tool for trace analyses, but requires in most cases at least microsampling. Only the classical, photon-excited methods allow raw materials of almost any kind and shape to be analyzed (as long as the sample fits into a sample holder or an open beam instrument is used). Both energy-dispersive and wavelength-dispersive modes are employed, but an important difference between these two is the primary radiative intensity. This can differ by a factor of 10 and more and should be taken into account in the case of sensitive materials.

Information depth

When radiation from a x-ray tube penetrates a specimen, it is absorbed along its path. A major fraction of the energy of the absorbed photons is converted into analytically useful fluorescent photons of the various atoms, and some of

them reach the surface of the specimen and the detection system. The observed intensity (more correctly, the number of observed photons) is a function of the composition of the specimen and its thickness. A layer of thickness

$$D = \frac{1}{\rho \left[\frac{\mu(E)}{\sin \psi_1} + \frac{\mu(K\alpha_1)}{\sin \psi_2} \right]}$$

emits about 63.2% of the fluorescent intensity of an infinitely thick bulk material, and correspondingly more for thicker layers (Table 1). In this equation, $\mu(E)$ and $\mu(K\alpha_1)$ are the (total) absorption coefficients of the sample for the incident photons (energy E) and observed fluorescent photons (assuming $K\alpha_1$), ρ is the density and ψ_1 and ψ_2 are the angles of the primary and fluorescent beams to the specimen surface, respectively. Secondary excitation effects may alter the value of D slightly.

In most cases, the experimental error in analyses of art objects exceeds 5%. It is then difficult to distinguish between a bulk material and a layer with a thickness of more than $3D$ and therefore reasonable to classify, arbitrarily, $D_{\text{inf}} = 3D$ as the information depth. This is, however, not a generally agreed definition, and providing a value of D should be preferred.

The absorption coefficients in the equation for D are a function of energy (E represents the energy of the tube photon and $K\alpha_1$ that of the fluorescent photons) and the composition of the sample with elements j :

$$\mu(E) = \sum_j c_j \mu_j(E) = c_i \mu_i(E) + c_M \mu_M(E)$$

$$\mu(K\alpha_1) = \sum_j c_j \mu_j(K\alpha_1) = c_i \mu_i(K\alpha_1) + c_M \mu_M(K\alpha_1)$$

where the subscript i represents the analyzed element and M the matrix. It is obvious that any large value of one of the coefficients decreases the information depth. Note that the energy E in the case of polychromatic radiation is a mean value within the integration interval and is not trivial to determine. A software utility to compute $\mu(E)$ for chemical formulae is available from the authors by E-mail to mmantler@xrm.atp.tuwien.ac.at (free of charge for educational and academic institutions).

In some cases elements are analyzed where two analytical lines of (very) different energies are available, in most cases a K- and an L-line (e.g. Cd $K\alpha$ and Cd $L\alpha$ in cadmium yellow/red/orange or Ba $K\alpha$ and Ba $L\alpha$ in manganese blue). Because of the much higher absorption of the L-lines due to their lower energy, their information depth is much lower; this can be sometimes used with advantage for the analysis of layered materials.

Table 1. Relative intensities compared with bulk material as a function of layer thickness

Thickness	% of bulk intensity
D	63.21
$2D$	86.47
$3D$	95.02
$4D$	98.17
$5D$	99.33

Table 2. Chemical composition of some pigments, usual mixing ratio with oil, absorbance (including binding medium) and density (without binding medium)^{30,31}

Pigment	Formula	Oil (g per 100 g pigment) ^a	D (μm) ^b	Density (g cm^{-3})
Lampblack, soot	C	60–90	1	1.65
Black iron oxide	$\text{FeO}\cdot\text{Fe}_2\text{O}_3$	30–55	15	4.2–4.5
Cobalt blue	CoAl_2O_4	40–75	22	3.25
Ultramarine blue	$\text{Na}_{6-8}\text{Al}_6\text{Si}_6\text{O}_{24}\text{S}_{2-4}$	25–55	1	1.9–2.5
Manganese blue	$\text{Ba}_3(\text{MnO}_4)_2\cdot\text{BaSO}_4$	10–20	7	4.15
Terra di Siena	Fe_2O_3	30–70	17	2.6–3.3
Umbra	$\text{Fe}_2\text{O}_3 + \text{MnO}_2$	25–70	19	2.5–3.2
Chromium oxide green	Cr_2O_3	15–40	10	4.7
Vermilion	HgS	12–30	6	8.0
White lead	$2\text{PbCO}_3\cdot\text{Pb}(\text{OH})_2 + 4\text{PbCO}_3\cdot2\text{Pb}(\text{OH})_2\cdot\text{PbO}$	9–25	8	6.81
Zinc white	ZnO	14–45	14	5.5
Titanium white	TiO_2	16–36	11	3.1–3.3
Cadmium yellow	$\text{CdS}: \text{Cd L}\alpha: \text{Cd K}\alpha:$	30–60	17	4.0
			123	

^a The lower number for the oil to pigment ratio is for a stiff paste and the higher number for a lighter bodied paint. An average value was used for computations.

^b Selected line: K α of heaviest element in pigment, except L α for Ba, Cd, Hg, Pb, Sn, or as indicated in the case of cadmium yellow. Computed for Rh target end-window tube, 40 kV, 63.5° and 45° angles of incident and observed radiation, respectively.

A special situation occurs when the absorption edge of a matrix element happens to have an energy between the K α and K β lines of an element. The K β /K α ratio of the element to be analyzed is then a sensitive function of the concentration of the absorbing matrix element.

Information depth in paint layers

Paints are made by mixing pigments with a liquid binding medium (e.g. drying oil). After applying a layer of paint, it is generally dried and eventually other layers are added as needed. A final coating of varnish often protects paintings. The thickness for the whole structure ranges from a few micrometers up to 1 mm or more. A list of some commonly used pigments and their chemical composition is given in Table 2.

Varnish and binding media consist of organic compounds (such as vegetable oils, egg yolk, egg white and resins) and thereby predominantly of light elements, which cause only modest absorption for the fluorescent radiation from the heavier elements. For numerical computations the absorption coefficient can be roughly approximated by that of water (Fig. 1).

Usually a pigment is analyzed by its heaviest element, but another selection may be advisable when other pigments containing the same element(s) must be distinguished. As can be seen from Table 3, the heaviest elements in a pigment have usually the highest concentration. Computed information depths $D_{\text{inf}} = 3D$ can be obtained from Table 2 and Fig. 2. These values vary considerably with the composition of the paint layer and the energy of the measured line. Because of the wide range of possible mixing ratios between pigment and oil and the varying densities of pigments and oils, the number obtained for the geometrical thickness of a layer may be rather uncertain. It should be noted that the drying process of an oil as a binding medium is a complex chemical

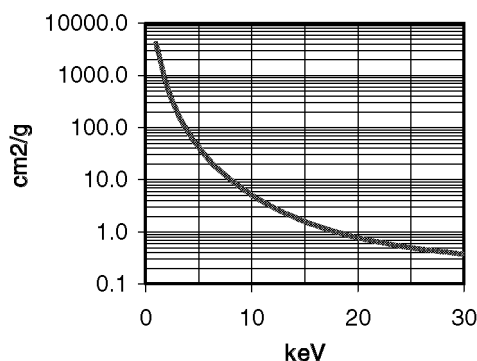


Figure 1. Absorption coefficient of water as a function of the photon energy. This can be used to approximate the absorption by the binding medium (oil) or varnish.

reaction with the ambient air, which is generally not associated with the evaporation of the medium, as for example in the case of animal glue and water. Nevertheless, some changes may take place in the density and thereby in the thickness of a layer.

Absorption by the matrix and interelement effects

Elements in the pigment and those in the medium contribute to matrix absorption. Secondary excitation by the binding medium is unlikely, because it consists mainly of light elements, but it is possible within a pigment and between elements of different pigments. As mentioned above, the mixing ratio of pigment and binding medium varies considerably. Naturally, lines with low photon energies (from light elements or L- and M-lines) are more strongly absorbed by the matrix and remain at a low level even for high concentrations of the pigment. As an example, the theoretical dependence of the Pb L α intensity from white lead on the concentration of the binding medium is shown in Fig. 3.

Table 3. Pigment and element concentrations in the paint layer^{30,31 a}

Pigment	Formula	Pigment (wt%)	Element (wt% in pigment)	Element (wt% in paint)
Lampblack, soot	C	53–63	C (100.0)	53–63
Black iron oxide	FeO·Fe ₂ O ₃	64–76	Fe (72.4)	46–55
Cobalt blue	CoAl ₂ O ₄	57–71	Co (33.3)	19–24
			Al (30.5)	17–22
Ultramarine blue	Na _{6–8} Al ₆ Si ₆ O ₂₄ S _{2–4}	64–80	Si (~28.7)	18–23
Manganese blue	Ba ₃ (MnO ₄) ₂ ·BaSO ₄	83–90	Ba (56.1)	46–50
			Mn (11.2)	9–10
Terra di Siena	Fe ₂ O ₃	59–77	Fe (69.9)	41–54
Umbra	Fe ₂ O ₃ + MnO ₂	59–80	Fe (~45.3)	27–36
			Mn (~22.3)	12–18
Chromium oxide green	Cr ₂ O ₃	71–87	Cr (68.4)	49–60
Vermilion	HgS	77–89	Hg (86.2)	66–76
			S (13.8)	11–12
White lead	2PbCO ₃ ·Pb(OH) ₂ + 4PbCO ₃ ·2Pb(OH) ₂ ·PbO	80–90	Pb (~81.3)	65–73
Zinc white	ZnO	69–88	Zn (80.3)	55–70
Titanium white	TiO ₂	74–86	Ti (59.9)	44–52
Cadmium yellow	CdS: Cd L _α : Cd K _α :	77–89	Cd (77.8)	59–69
			S (22.2)	17–20

^a Pigment and element concentrations vary with oil contents as defined in Table 2.

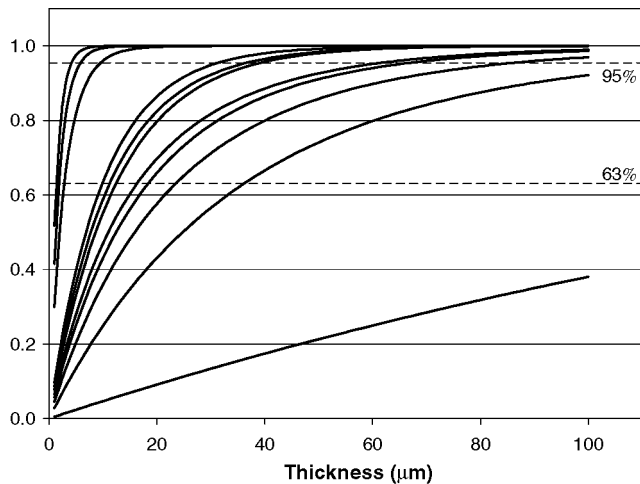


Figure 2. Computed intensities from paint layers (pigments and binding medium) as a function of layer thickness for several pigments. The intensities are normalized to those from bulk materials. From left/top to right/bottom: lamp black, C K_α; ultramarine, Al K_α; cadmium yellow, Cd L_α; vermillion, Hg L_α; cobalt green, Zn K_α; white lead, Pb L_α; chromium oxide green, Cr K_α; titanium white, Ti K_α; zinc white, Zn K_α; cobalt blue, Co K_α; cadmium yellow, Cd K_α.

The effect of the matrix elements, j , on the analyzed element, i , is often described by the α coefficients in the empirical parameter equation $c_i/R_i = 1 + \sum_{j \neq i} \alpha_{ij} c_j$, which is also widely used to compute concentrations c_i from count rate ratios R_i . It can be simplified to $c_i/R_i = 1 + \alpha_{iM} c_M$, where M denotes the general influence of the matrix. The ideal situation is $\alpha_M = 0$ (neutral matrix) and consequently $R_i = c_i$; if α_M is a positive number, lower count rates must be expected ('absorbing matrix'), while negative numbers indicate higher count rates ('enhancing matrix').

Table 4 summarizes the effect of some combinations of pigments including a binding medium. Note the strong

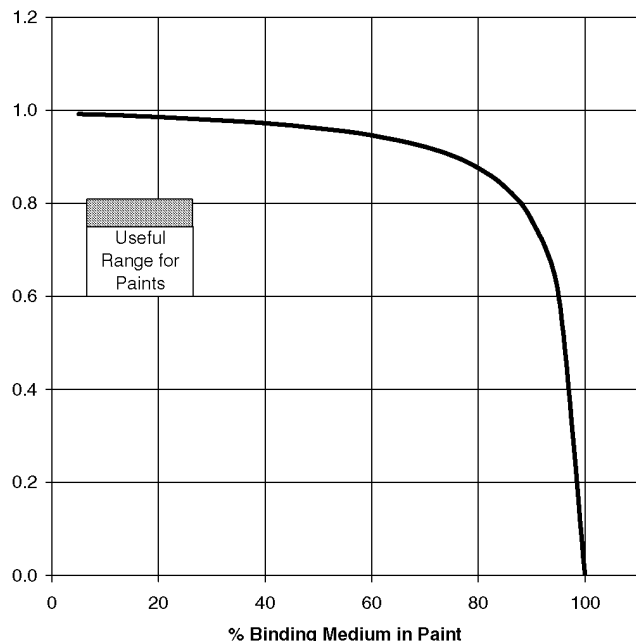


Figure 3. Intensity of Pb L_α radiation from a paint as a function of binding medium in the paint. The absorption properties of the binding medium are approximated by those of water (Fig. 1). The intensity values are normalized to the pure pigment.

absorbing effect of white lead, which is often mixed with other pigments.

Homogeneity of the system pigment–binding medium

The size of pigment grains is around 1 μm, depending on the manufacturing process; historical pigments are often much larger and those made by modern industrial producers sometimes much smaller. The limited number of Monte Carlo simulations carried out so far on such

Table 4. Computed matrix effects within the paint layers

Line	Matrix	Concentration of analyte element (wt%)	Rel. intensity ^a	α_M	Matrix is
Pb L α	White lead	72	0.99	-0.97	Enhancing
Zn K α	Zinc white	69	0.96	-0.91	Enhancing
Ti K α	Titanium white	45	0.75	-0.72	Enhancing
Fe K α	Black iron oxide	60	0.91	-0.85	Enhancing
Co K α	Cobalt blue	26	0.56	-0.72	Enhancing
Al K α	Cobalt blue	24	0.11	1.46	Absorbing
Mn K α	Manganese blue	8.6	0.04	1.08	Absorbing
Ba L α	Manganese blue	43	0.77	-0.78	Enhancing
S K α	Manganese blue	5.0	0.044	0.30	Absorbing
Hg L α	Vermilion	76	0.95	-0.84	Enhancing
S K α	Vermilion	12	0.024	4.55	Absorbing
Fe K α	50% black iron oxide, 50% white lead	30	0.22	0.48	Absorbing
Pb L α	50% black iron oxide, 50% white lead	36	0.55	-0.54	Enhancing

^a Relative to pure element.

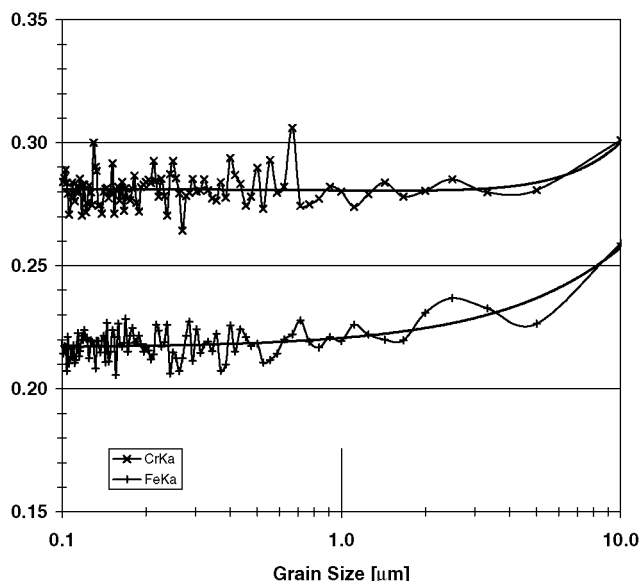


Figure 4. Intensity of Fe K α and Cr K α from grains as a function of grain size. Dilution in binding medium and using oxides (pigments) would reduce the dependence. The statistical deviations of the data points are a result of a Monte Carlo simulation.

systems suggest that the error introduced by this inhomogeneity is low (Fig. 4) and usually need not be taken into account unless the average grain size exceeds about 5 μm (depending on the matrix).³²

Destructiveness of XRF and radiation damage

A very important aspect of applying an analytical technique to the analysis of objects of art and archaeology is its degree of non-destructiveness. XRF is usually seen as a non-destructive method, but the exact meaning of this term must be clarified. For the analyst the specimen is a small piece of material, which may have at least required cutting into shape to fit into a specimen holder, and has possibly undergone also further treatment by cleaning, polishing,

coating, etc. If the analytical procedure does not alter such a specimen, it is said to be non-destructive. Nevertheless, the process of taking a specimen from an object may be a destructive step by itself and unacceptable from the viewpoint of an art historian, archaeologist or conservator.

Several x-ray spectrometers have been built which can analyze small areas of large objects without the necessity to remove any material or even touch the object. Their disadvantage is that they are limited in the elements that can be analyzed in air (or under a protective, light gas) and surface contamination and roughness may affect the quality of quantitative analyses.^{33,34}

Radiation damage by x-rays is observed when the chemical state of atoms (bound to other atoms) in the specimen is permanently altered by radiative energy. In general, the process is cumulative and its effect approximately a function of the product of photon flux, time and the particular photon energy, i.e. of the absorbed radiative dose. It is not limited to x-rays and can often occur by illumination with any other intense electromagnetic radiation, particularly by visible and ultraviolet light (natural daylight). A short duration of exposure to x-rays is therefore not necessarily more harmful than exposure to natural light over many years.

The most visible effect of a high radiation dose in many materials is a permanent or temporary darkening of the irradiated area. This is by no way restricted to organic compounds and can be observed, for example, at a polished copper surface or at most (transparent) glasses. Organic materials are, however, particularly sensitive and, besides darkening (yellowing), they may even visually decompose and become mechanically brittle. Both effects are observed, for example, after prolonged exposure of white fabrics to x-rays. Sometimes a 'healing effect' is reported, which reverses the yellowing after some time.

With the instrument with an open beam (see Fig. 8) used by one of the authors (M.S.), the maximum energy of the x-ray tube is 2.8 kW at 60 kV with most measurements carried out at 50 kV and 10 mA (0.5 kW) and an acquisition time for one spectrum of 30 s. No radiation damage could be observed at any object analyzed in the 8 years of operation.

CASE STUDIES

The following examples illustrate some applications of XRF to the analysis of art objects and we attempt to explain the goal of the investigations and the advantages and limitations of x-ray analysis.

Identification of pigments in paint layers

The identification of pigments present in an easel painting or polychromed sculpture is traditionally carried out by means of light microscopy. For this purpose a cross-section of a properly sampled specimen has to be prepared, which makes the analysis destructive in the sense that the original object is affected. The guiding principle for taking samples is to obtain an undamaged splinter, where the sequence of all paint layers is preserved. In the case of valuable objects of art, the size of the specimen must be limited to an absolute minimum. Tools for obtaining such splinters are eye scalpels, lancet needles and dissecting needles. Generally applicable recommendations cannot be given, since the success of sampling depends on the thickness and brittleness of the paint layers.

The preparation of a cross-section follows metallographic procedures, where the sample is embedded with a particular orientation in a transparent resin, which sets without shrinkage and penetrates only the outer domain of a specimen. Breaking out during grinding and polishing is thereby minimized. By using polarized light and the dark-field reflectance technique in a light microscope, such a

cross-section reveals information about the sequence and thickness of paint layers, grain size and grain size distribution of the pigments. These are useful indicators as modern pigments show a very uniform distribution of their grain size, whereas hand-ground materials are strongly heterogeneous. In addition, the presence of extender pigments, varnish layers or retouches after conservation treatments can easily be detected. Metallic foils of gold, silver or precious alloys, often used on polychromed sculptures, can be seen clearly, although their thickness is sometimes less than 1 µm. In addition to stratigraphic analyses, single pigment grains can be identified by comparing their color with those of standard materials or using, for example, SEM-EDX. For this purpose the cross-section has to be coated with a thin carbon layer in order to reduce charging effects, which occur during the electron bombardment. The size of such cross-sections including the support is in the range of less than 1 in so that they can be placed easily into the SEM sample chamber; such investigations are non-destructive for the specimen and further studies can be carried out afterwards.

A micrograph of a paint layer cross-section is shown in Fig. 5. It is the section of a polychromed sculpture of the 16th century with vermilion mixed with white lead on the top (layer 1) followed by a layer of pure white lead (layer 2) and a layer of red lead mixed with white lead (layer 3). Underneath these paint layers again a thick white layer (layer 4) consisting of white lead followed by a gray layer of carbon black mixed with white lead (layer 5) and several layers of verdigris mixed with different amounts of white lead (layer 6) can be seen.

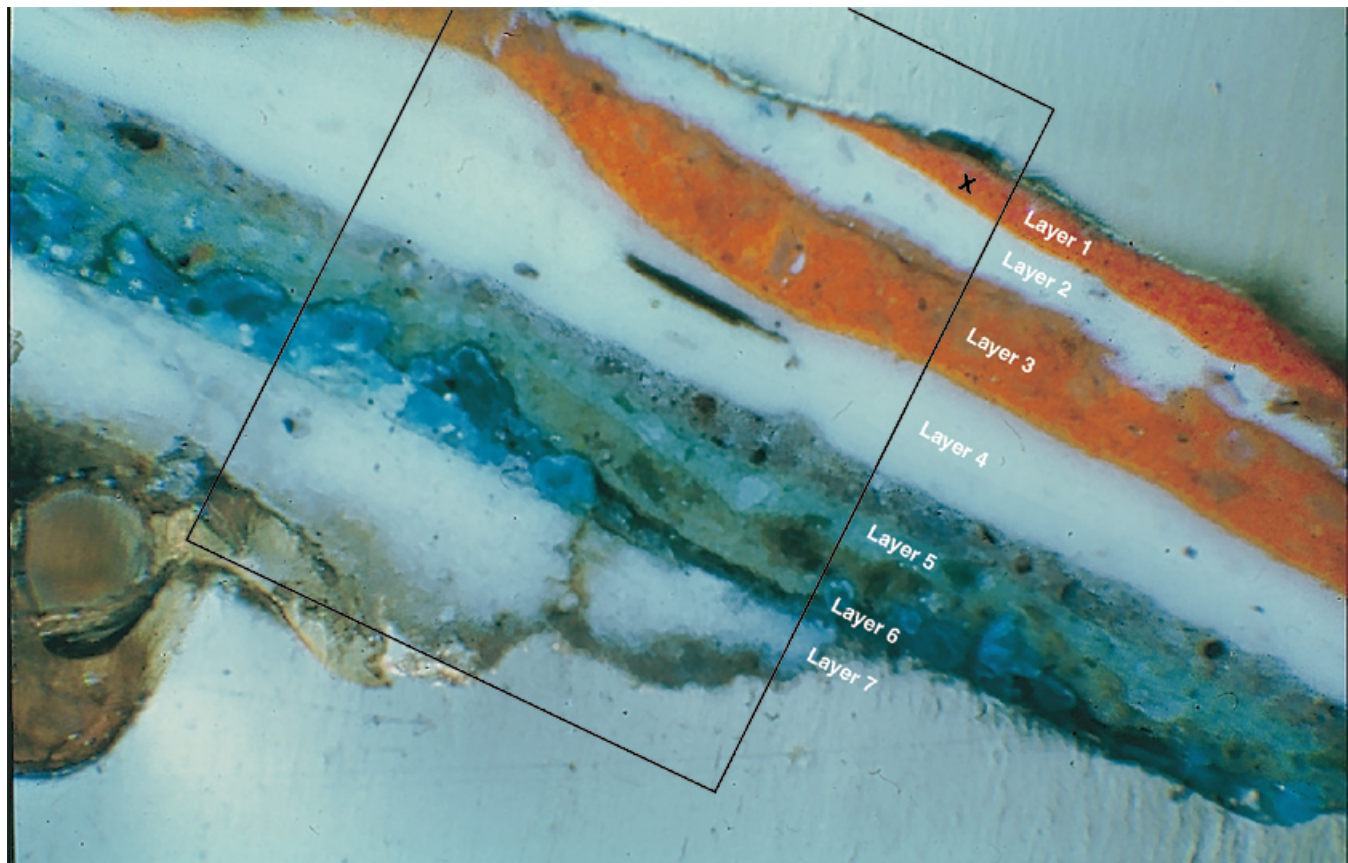


Figure 5. Cross-section of paint layers of a polychromed sculpture of the 16th century.

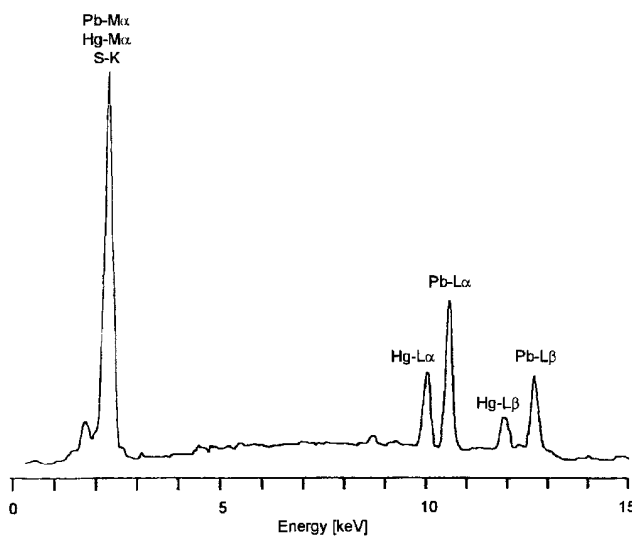


Figure 6. Result of the SEM-EDX obtained for the red paint layer.

As ground material, a thick layer of chalk (layer 7) was applied on the wooden support. Additional information

about the element distributions as obtained by SEM-EDX is summarized in Figs 6 and 7. Figure 6 shows the result of point analysis in layer 1, where the elements Hg, Pb and S could be detected. In Fig. 7, the backscattered electron image and the corresponding elemental distributions of Pb, Cu and Ca can be seen.

Shielding effects by coatings (varnish) and by other paint layers. The paint structure shown in Fig. 5 is used to illustrate the effect of shielding the fluorescent radiation from a paint layer by others. The simplified model assumes layers with equal, constant thicknesses (Table 5). It is obviously impossible to distinguish between the lead in layers 1–6 and the data for Pb L α reflect a sum over all of them. Hg L α from the top layer depends on the layer thickness up to saturation at around 20 μm ; the shielding by mercury also affects the lead photons from layers 2–6 and decreases their total intensity with increasing thickness of the top layer. Cu K α photons from layer 6 are faintly visible, as long as layers containing white lead are extremely thin. Ca K α from layer 7 cannot be measured at all.

Small splinters as used for the example above cannot be measured with conventional XRF instrumentation. In

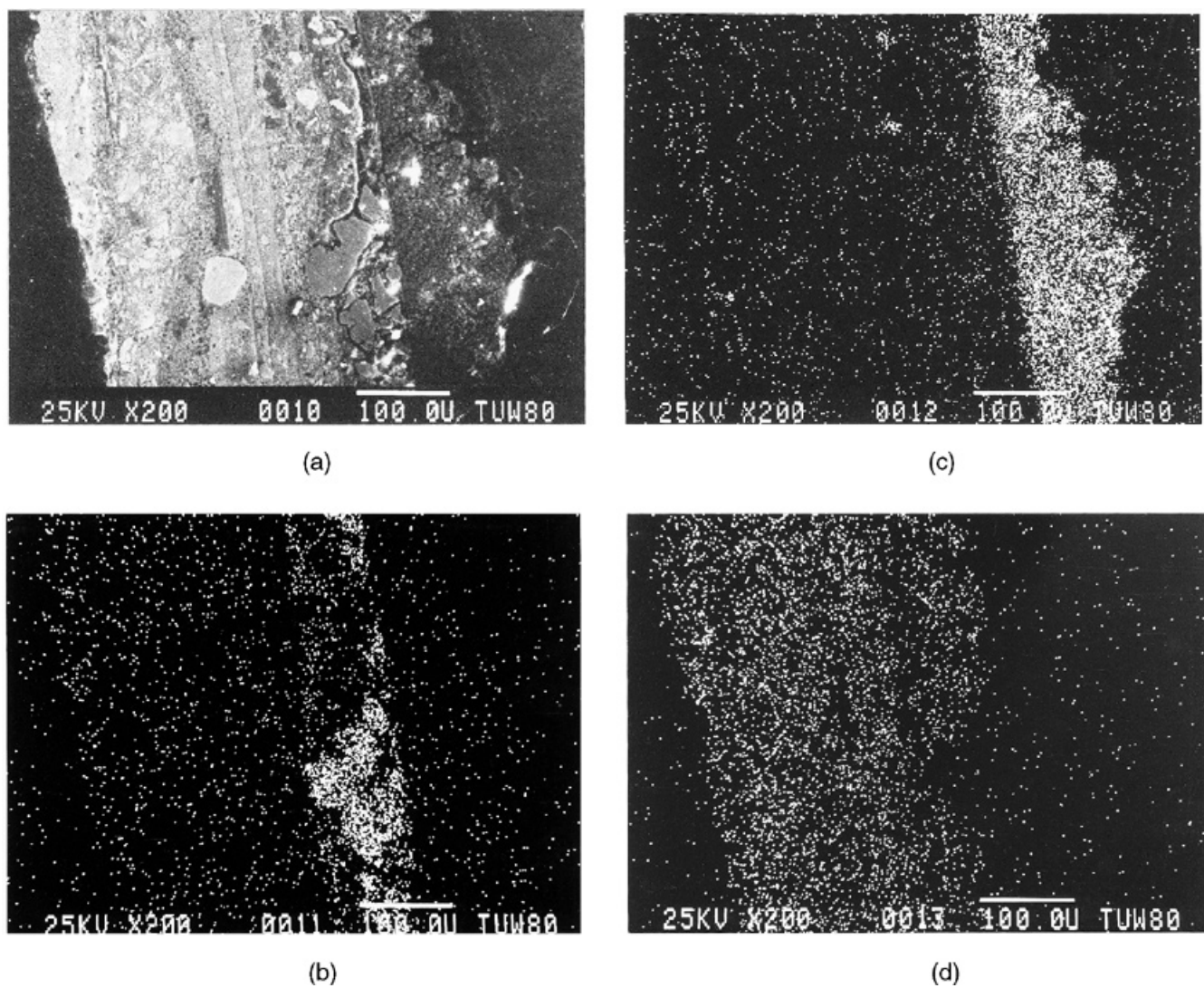


Figure 7. Detail of Fig. 5 seen in the backscattered electron mode in the SEM (a) and the corresponding elemental distributions of Cu (b), Ca (c) and Pb (d).

Table 5. Theoretically obtainable information by XRF from the sample shown in Fig. 5: top, composition of each layer; bottom, computed intensities (relative to pure, infinitely thick element) from the layer structure^a

Layer 1	Vermilion + white lead	Hg, Pb		
Layer 2	White lead	Pb		
Layer 3	Red lead	Pb		
Layer 4	White lead	Pb		
Layer 5	Carbon black + white lead	Pb, C		
Layer 6	Verdigris + white lead	Pb, Cu		
Layer 7	Chalk	Ca		
	2 μm	20 μm	50 μm	100 μm
Hg L _α	0.1492	0.5041	0.5244	0.5246
Pb L _α	0.6329	0.5138	0.4858	0.4853
Cu K _α	0.0026	0		
Ca K _α	0			

^a All layers are assumed to have the same indicated thickness.

order to study the influence of the shielding effects by a thin paint layer consisting of pure white lead experimentally, an x-ray spectrometer designed at the Academy of Fine Arts in cooperation with the Institute of Applied and Technical Physics at the Vienna University of Technology was employed. This instrument is based on energy-dispersive XRF analysis and enables pixel-by-pixel analysis along lines or within selected areas.³⁵ It consists of a spectroscopic x-ray tube, an Si/Li detector and additional

devices all mounted on a support system, which can be moved in three dimensions in order to select the pixels to be measured and to adjust the distance between the measuring system and an object. The whole system is shown in Fig. 8 with the frame, where large objects such as an easel painting up to 2 × 3 m can be mounted vertically. During the analysis, the object is fixed and various preventive measures are taken in order to minimize the danger of any damage during the examination. The instrument is

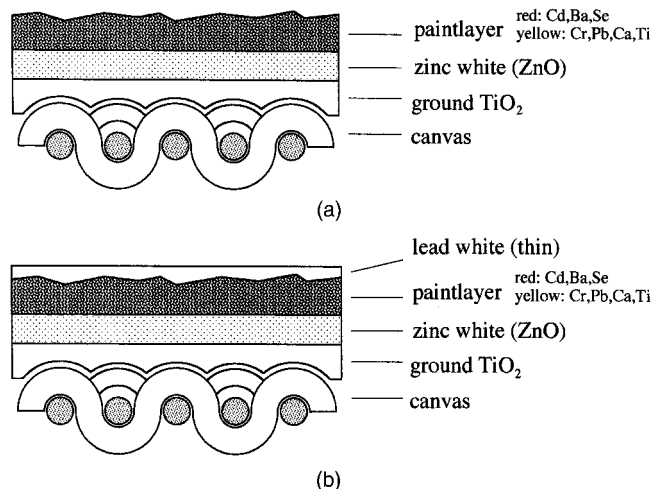


Figure 9. Scheme of the paint layer structure of an easel painting measured with the pixel-by-pixel XRF. The elemental distributions were measured before (a) and after (b) coating the paint layer with a thin layer of lead white.

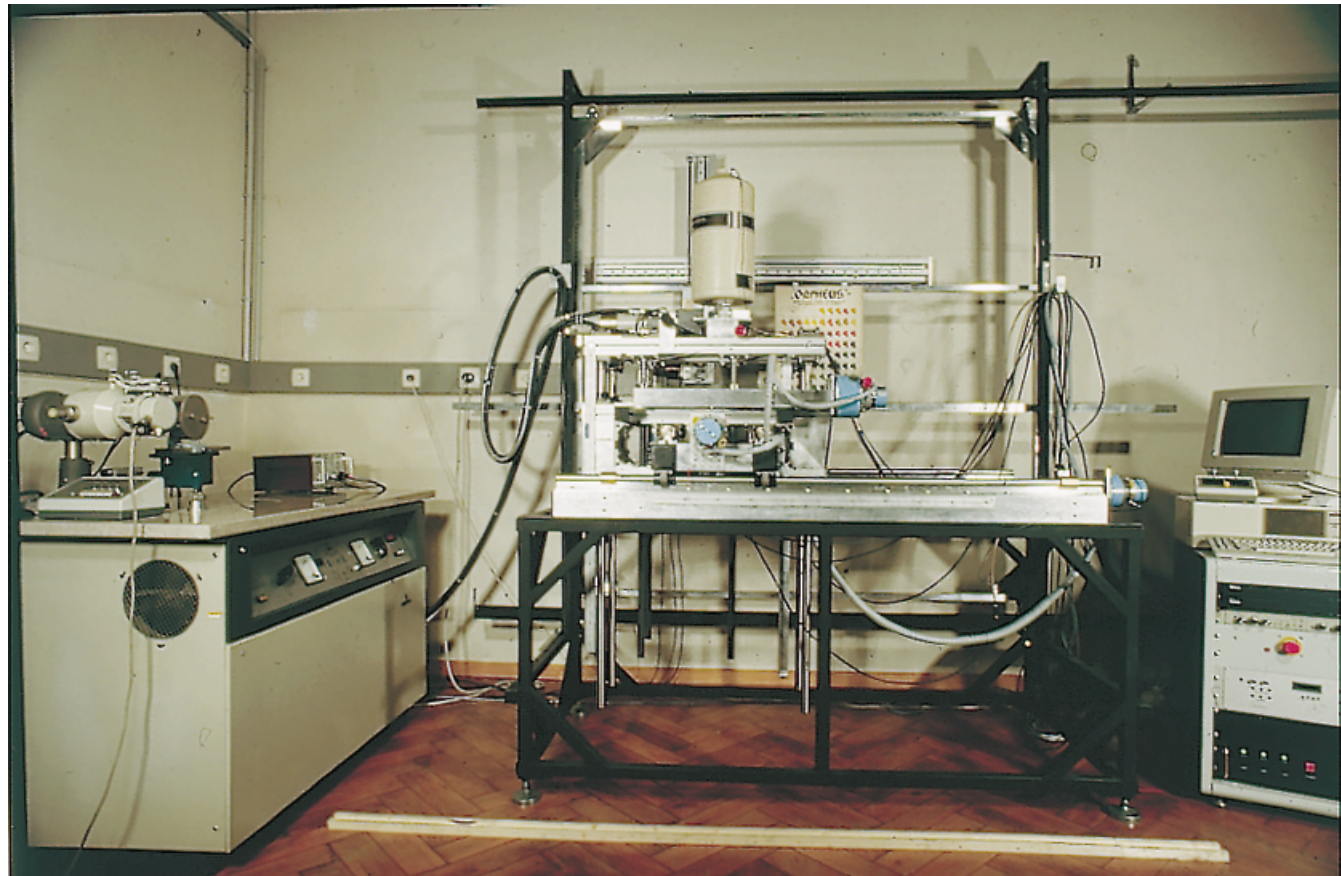


Figure 8. Pixel-by-pixel XRF for non-destructive determination of the material composition of large artifacts.

located in a separate room with brick walls at least 0.5 m thick in order to protect the operator and the environment from x-radiation.

Figure 9(a) shows the scheme of paint layers with pigments containing various elements such as Ca, Ti, Cr, Zn, Se, Cd, Ba and Pb. On the canvas support two layers,

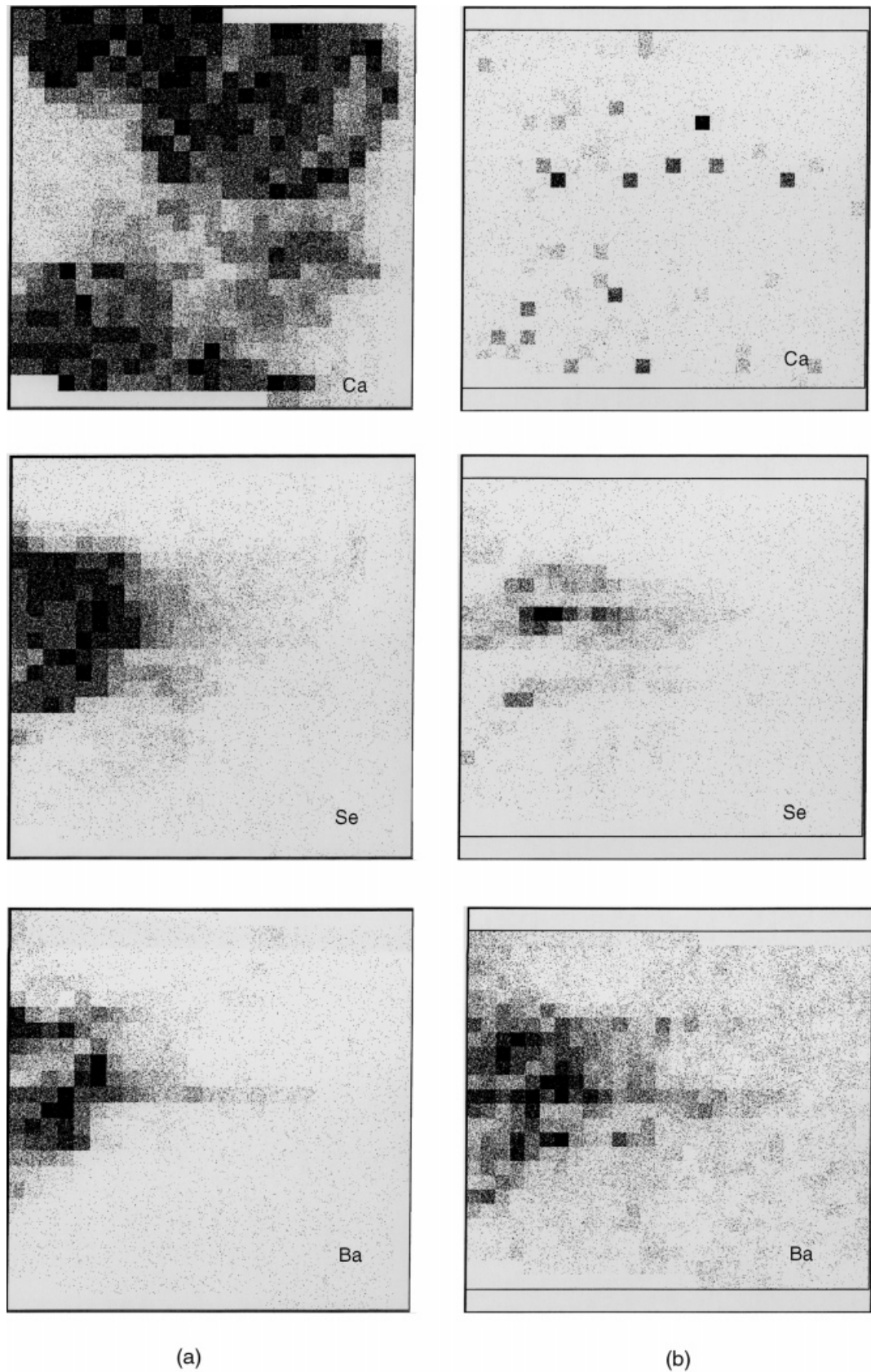


Figure 10. Elemental distribution of the elements Ca, Se and Ba before (a) and after coating the paint layer with a thin layer of lead white (b).

titanium white and zinc white, respectively, were applied by a trained artist as evenly as possible with conventional tools (brushes). Then the ZnO layer was coated side by side with red paint (pigments containing Cd, Se, and Ba) and yellow paint (Cr, Pb, Ca, and Ti). Their elemental distributions were measured by the pixel-by-pixel XRF instrument before [Fig. 10(a)] and after [Fig. 10(b)] applying a final thin paint layer (of approximately 10–15 µm thickness) of white lead [Fig. 9(b)].

The fluorescent radiation from the elements with medium atomic numbers such as Ca, Ti, Cr or Zn is readily visible on the painting without white lead and can be used to obtain information about their spatial distribution. From

the second painting, with a layer of white lead, only the fluorescent lines with higher energies, Cd K α and Ba K α are detectable, all other being absorbed by lead.

Pigments in illuminated manuscripts

In contrast to the complex layer structure in Figs 5 and 9, miniature paintings on parchment usually consist only of two or even one thin paint layer. Such an object, a patent of nobility dated at the end of the 18th century, is shown in the Figs 11 and 12. It represents a coat of arms flanked by two caryatids. The portraits of two sovereigns are painted in the upper corners and the inscriptions IHS



Figure 11. Patent of nobility with a miniature painting on parchment of the 18th century.

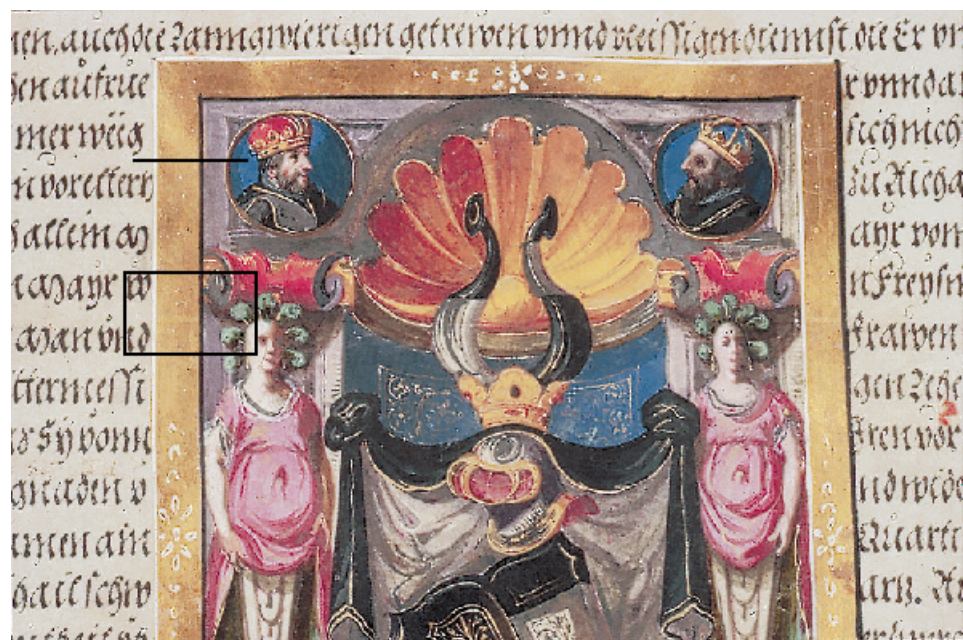


Figure 12. Detail of Fig. 11 showing the line and the rectangular area where the elemental distributions were determined (see Figs 13 and 14).

and MARIA are in the lower left and right corners, respectively. Between the inscriptions the coats of arms of the Austrian Empire and the Dukedom of Tyrol, part of the Habsburg Monarchy, can be seen. It is not surprising that very few technical analyses have been carried out on such miniature paintings. The scale of such art objects presents problems in examination, and it is usually impossible to take even small samples for analysis. In order to analyze the pigments, pixel-by-pixel analyses along the line and within the selected area indicated in Fig. 12 were carried out in order to determine the distributions of the characteristic elements.

The palette of materials used in the miniature painting is summarized in Table 6. Gold leaf and silver powder were used for the golden frame and the gray parts of the coats of arms. The yellow decoration on the gold was painted by using orpiment (King's yellow) containing arsenic and sulfur. Only arsenic could be detected by the energy-dispersive spectrometer, since the fluorescent radiation from sulfur is strongly absorbed by the air. In the red parts of the miniature painting mercury indicates the presence of vermillion (HgS). It is one of the disadvantages of all x-ray analysis systems operating in air that the light elements such as C, N, O, Na, Mg, Al, Si, and S can hardly be detected.

The question of whether malachite (Cu carbonate) or verdigris (Cu acetate) was used cannot be clearly answered by energy-dispersive analysis. In such cases microscopic investigations and x-ray diffraction analyses are required to identify the pigments.

The results also reveal that the pigments were applied as pure materials and were not mixed with white lead or chalk as known from easel paintings. The small amounts of calcium and iron found in all the spectra were also detected in the unpainted parchment, indicating that their concentrations in the pigments could be negligible. On the other hand, large amounts of calcium and iron were determined in the area of the golden frame due to the red bole beneath the metallic layer.

The results in Table 6 could be confirmed by line scans and scans within the selected region indicated in Fig. 12. An area of approximately $12 \times 20 \text{ mm}^2$ and a line of 25 mm were measured using the area and line scan features of the pixel-by-pixel x-ray spectrometer. The pixels were set at 1 mm apart and an acquisition time of 30 s was used for each spectrum. The instrument requires a further ca 30 s for each positioning and data manipulation. Therefore, a total analysis time of 30 min for the line scan in Fig. 13 and 3.5 h for the area scan (Fig. 14) was required. An energy window (ROI) was set

Table 6. Results of the qualitative analysis carried out by x-ray spectrometry on a miniature painting on parchment

Color	Detected elements	Pigment
Gold	Au, Fe, Ca	Gold with red bole underneath
Grey	Ag, (Ca, Fe)	Silver
Yellow	As, (Ca, Fe)	Orpiment: As_2S_3
White	Pb, (Ca, Fe)	White lead: $2 \text{ PbCO}_3 \cdot \text{Pb(OH)}_2$
Red	Hg, (Ca, Fe)	Vermilion: HgS
Blue	Cu, (Fe, Ca)	Azurite: $2 \text{ CuCO}_3 \cdot \text{Cu(OH)}_2$
Green	Cu, (Ca, Fe)	Malachite or verdigris?

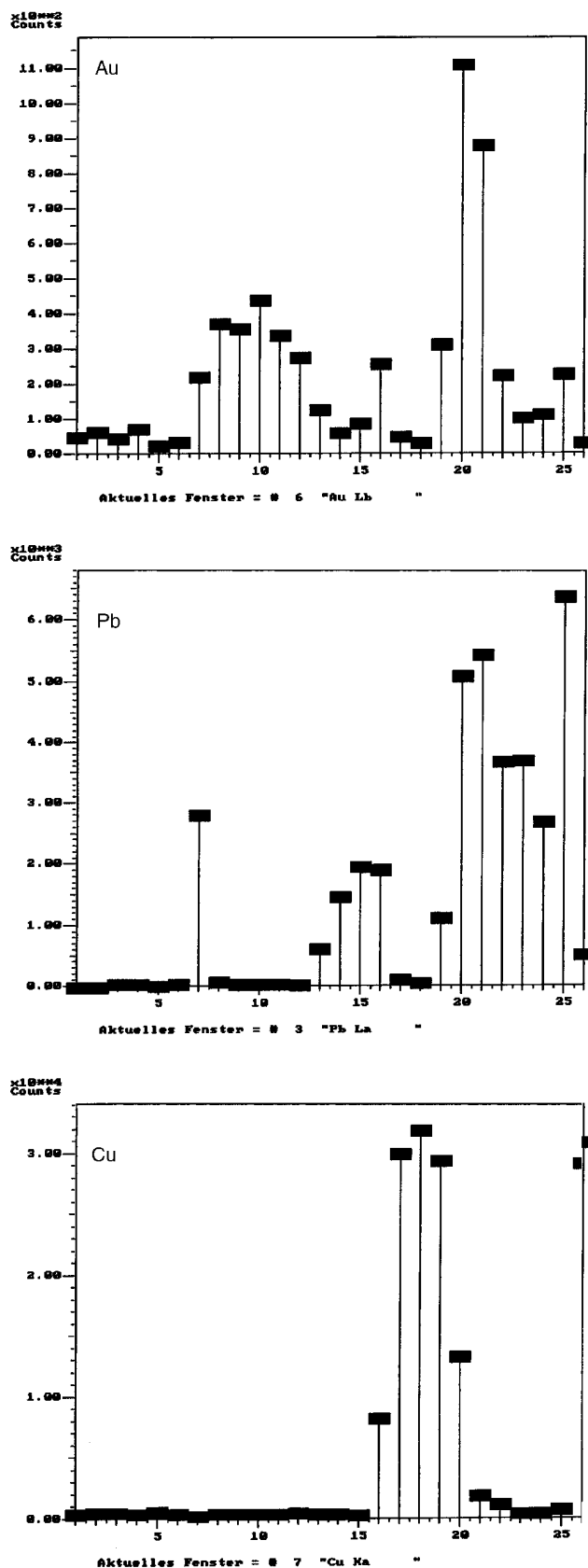


Figure 13. Line scan of Au, Pb and Cu along the line indicated in Fig. 12.

for each element of interest and a background subtraction was carried out using a third-order polynomial fit. This procedure was automatically repeated for all 240 spectra

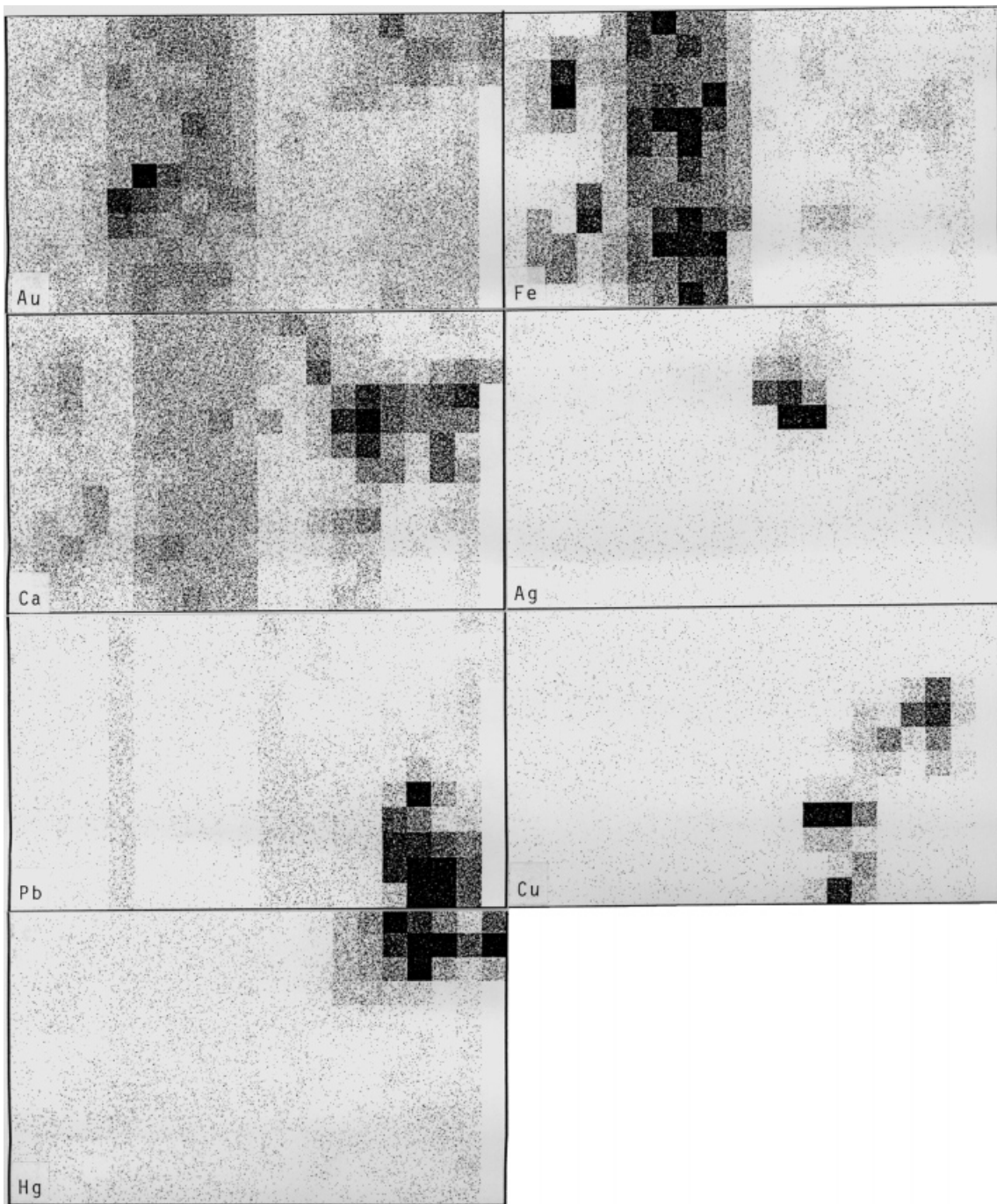


Figure 14. Elemental distributions of Au, Fe, Ca, Ag, Pb, Cu and Hg within the area indicated in Fig. 12.

of the area and the 26 spectra (including the end-point) of the line scan. The result is a data file containing the coordinates of each pixel with the net intensities of all the selected elements.

The line scans in Fig. 13 reveal the corresponding distributions of Au, Pb and Cu. Gold is present in the golden frame and the crown of the sovereign. The white line of the frame consists of white lead, which was also used for the carnation. The blue background in the portrait of the sovereign was painted with azurite.

The distributions of the various elements over the selected area are summarized in Fig. 14. It is evident that calcium and iron are present in the silica clay (red bole) beneath the gold layer. Calcium was also determined in

the gray parts containing silver. The text was written with an iron-containing material. The carnation of the caryatids was painted using white lead similar to the case for the portrait of the sovereign; the green decoration of the head contains copper. Mercury (vermilion) is present in the red parts of the column (capital).

Analysis of iridescent glass artifacts

Iridescent art glass is remarkable for the visual power it exerts through the splendid rainbow color gleam of its surface. Iridescence in itself is an interference effect occurring whenever a reflecting bulk material is coated

by a very thin layer with a refractive index different from that of the bulk. Archaeological glass objects sometimes appear to be iridescent due to leaching phenomena resulting in a several micrometer thin porous gel layer at the glass surface. In many cases, the adherence of this surface layer to the bulk glass is low and often it can be destroyed by a hand touch.

Apart from iridescent Islamic ceramics of the 13th century, no techniques for producing iridescent surfaces were available until Louis Comfort Tiffany's patent in 1881.³⁶ Several centers in Europe followed and the highest quality was achieved in Bohemia, at that time part of the Austro-Hungarian Empire.³⁷ J. Loetz Wwe. of Klostermühle (patent 1898) started an intensive production of art iridescent glass with exceptional quality around 1900. Although influenced by Tiffany glass, Loetz artifacts were not the result of an imitation but rather of a parallel development due to alternative technological approaches.^{36–38}

Since this type of glass started to be produced, Art Nouveau iridescent glass has been of great interest both for applied art museums and for private collectors. Numerous European and North American museums and private collectors possess splendid collections of this type and tend to extend them. In the classification of such objects mainly aesthetic and stylistic evaluations are applied, as already mentioned above. Scientific techniques based on material analysis have been rarely discussed so far, as these objects require non-destructive techniques and any sampling or changing of the glass material during the analysis must be avoided.

The goal of a joint research project of the Museum of Applied Arts in Vienna, the Austrian Research Center Seibersdorf and the Academy of Fine Arts, Vienna, in cooperation with Vienna University of Technology is to develop a 'recognition' procedure based on non-destructive analytical techniques supplemented with efficient experimental data processing, that would allow quick and reliable identification of the provenance of Art Nouveau iridescent glass objects. Within this project fragments of Loetz and Tiffany glasses and half products available in the Museum of Applied Arts in Vienna and the Historical Society in New York have been investigated. XRF and Fourier transform infrared (FTIR) methods were applied without sampling. In some cases cross-sections of a small glass splinter gained from the fragments could also be prepared and the structures studied by means of light microscopy and SEM-EDX.

The vase shown in Fig. 15 is an intact artifact made by Loetz. A cross-sectioned glass fragment made from similar material was analyzed (Fig. 16), where the bulk glass has a thickness of 2.5–3 mm and is coated with an iridescent layer of 360–430 µm. SEM-EDX revealed that the main elements in the bulk material are potassium, calcium, silicon and oxygen, whereas the iridescent layer contains silver in addition and also large amounts of lead. Table 7 summarizes the chemical composition obtained by SEM-EDX and XRF.

Because silver and lead are only present in the iridescent layer, thickness determination is in principle possible via the Pb L α , Pb L β , and Ag K α lines when excited by photons, but not with electron-excited XRF because of the limited pathlength of electrons in the sample. The most accurate approach (used in this study) is,

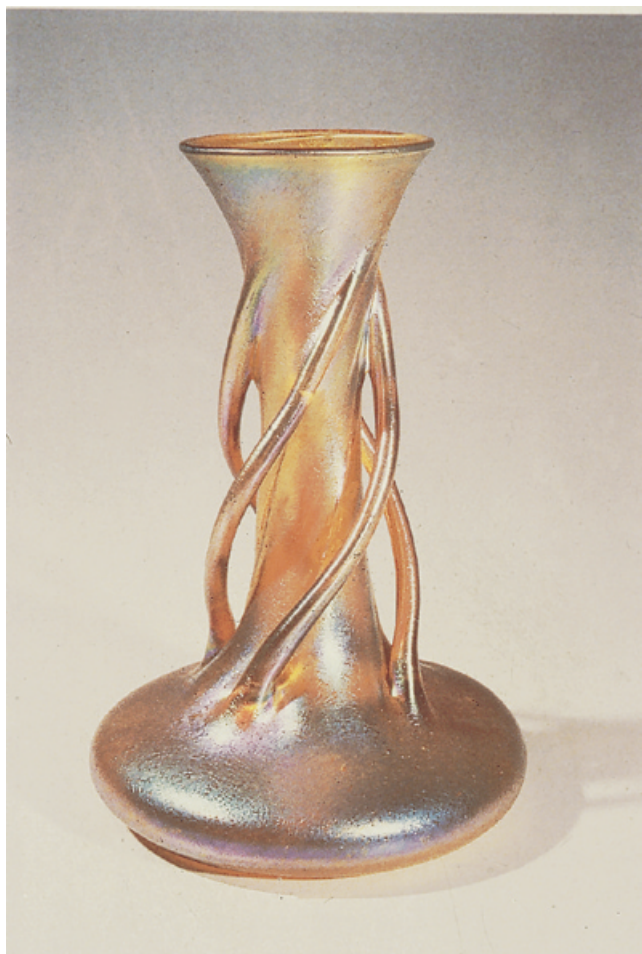


Figure 15. Art Nouveau glass artifact manufactured by Loetz.³⁶

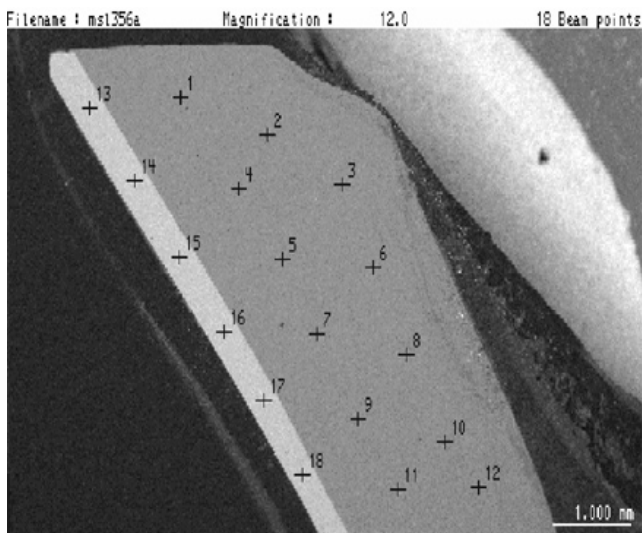


Figure 16. Cross-section of a Loetz glass fragment seen with SEM. The bulk glass consists of a potash-lime-silica glass, which was coated with a lead-containing glass (points 13–18) in order to achieve the iridescent effects.

of course, to measure the SEM image. In most investigated Tiffany glasses this was the only possibility, because lead and silver are also found in the bulk glass in comparably high concentrations as in the iridescent layer.

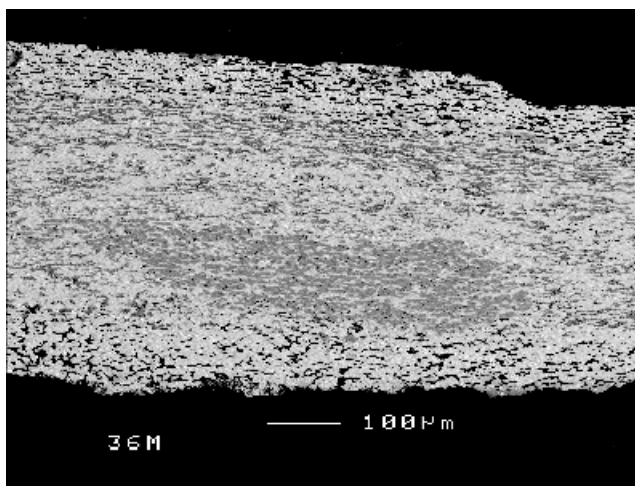
Analysis of medieval silver coins

XRF analysis has been widely used for the material analysis of coins as most of the objects can be analyzed in a non-destructive way even with commercially available instruments.^{39,40} As most such objects have been buried in the ground or even in the sea for centuries, corrosion phenomena must be observed on their surfaces. In Fig. 17 a set of coins consisting of an Ag–Cu alloy are shown

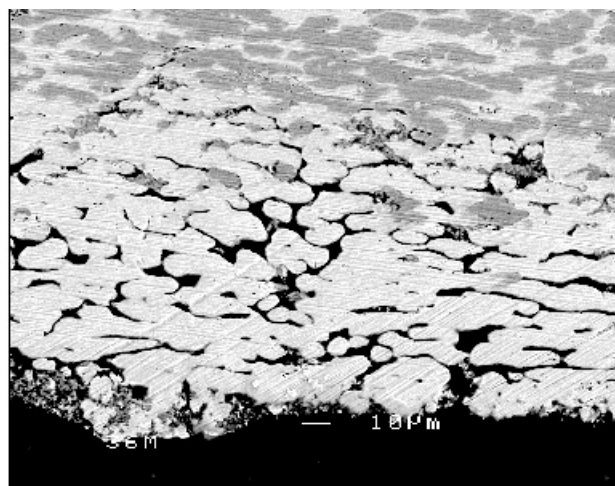
immediately after their excavation. The typical green patina on the surface of these objects is a consequence of a leaching process of copper (less noble than silver), whereas Ag has been enriched compared with the bulk. This phenomenon can be studied by means of SEM on a coin polished on its edge. Figure 18 illustrates the depletion of the copper-rich phase and the relative enrichment of the silver-rich phase on the surfaces of the coin. XRF measurements yielded a silver content of



Figure 17. Silver coins (Tiroler Kreuzer) after their excavation in St Valentin, Lower Austria, showing the typical green patina due to corrosion phenomena.



(a)



(b)

Figure 18. Cross-section of a silver coin showing the bright Ag-rich and the gray Cu-rich phases in the backscattered electron image (a). Additionally, a depletion of the copper-rich phase must be determined at the surface of the coin (b) yielding a relative enrichment of silver in the XRF analysis.

Table 7. Chemical composition of an iridescent Loetz glass artifact (sample L356)

Material	Na	Si	Cl	K	Ca	Ag	O	Pb	wt%
Bulk glass	2.4	34.3	0.4	12.0	5.4		44.7	0.4	
Iridescent layer	2.0	30.7	0.7	11.0	0.6	1.1	39.5	14.4	

$79.0 \pm 0.8\%$ Ag, whereas by SEM-EDX of an area of approximately $71 \times 55 \mu\text{m}$ a chemical composition of $43.9 \pm 0.7\%$ Ag and $55.7 \pm 0.6\%$ Cu could be determined for the bulk. The silver content determined by point analysis in the surface region, shown in Fig. 18(b), is $95.0 \pm 5\%$.

CONCLUSION

XRF analysis is a powerful and widely used tool, which has been successfully applied to many analyses of objects

in art and archaeology. It is non-destructive in the sense that a prepared specimen is usually not altered by the analytical procedure and with special instruments it is possible to analyze objects without taking samples and without physical contact. All modern methods of fundamental parameter computations including those for thin-film and multiple thin-film analyses and also Monte Carlo techniques for inhomogeneous specimens can be employed and reveal information that is otherwise inaccessible unless destructive methods and/or sampling material from the object are accepted.

Acknowledgements

The authors express their sincere thanks for providing objects for analyses and analytical data and figures particularly to Professor Mag. Karin Troschke (miniature painting), Dipl. Ing. Robert Linke (silver coins) and Dubravka Jembrih (iridescent glass), Academy of Fine Arts Vienna. The case studies are the result of fruitful cooperation with the Museum of Applied Arts Vienna (Dir. P. Noever, Dr W. Neuwirth and Mag. M. Trummer) and the Kunsthistorisches Museum Vienna (Doz. Dr M. Alarm, Mag. H. Winter). Dr Waltraud Neuwirth is also acknowledged for her permission to use Fig. 15.

REFERENCES

- M. H. Klaproth, *Abh. Königl. Akad. Wiss. Schönen Künste Berlin, Teil Exp.-Philos.* 1792–1797 3 (1795).
- M. H. Klaproth, *Abh. Königl. Akad. Wiss. Schönen Künste Berlin, Teil Exp.-Philos.* 1792–1797 72 (1795).
- M. H. Klaproth, *Abh. Königl. Akad. Wisse. Schönen Künste Berlin, Teil Exp.-Philos.* 1798–1800 31–40 (1798).
- M. H. Klaproth, *Gehlens J. Chem. Phys. Mineral.* **4**, 351 (1807).
- H. Raehlmann, Thesis, Berlin (1910).
- A. P. Laurie, *Analyst* **58**, 468 (1933).
- A. Eibner, *Mouseion* **29–30**, 113 (1935).
- R. J. Gettens, *Technical Stud. Field Fine Arts* **5**, 18 (1936).
- H. Malissa, *Mikrochemie* **35**, 34, 302 (1950).
- J. Plesters, *Stud. Conserv.* **2**, 110 (1956).
- H.-P. Schramm and B. Hering, *Historische Malmaterialien und Ihre Identifizierung*. VEB Deutscher Verlag der Wissenschaften, Berlin (1989).
- F. Feigel, *Spot Tests in Inorganic Analysis*. Elsevier, Amsterdam, (1954).
- F. Feigel, *Spot Tests in Organic Analysis*. Elsevier, Amsterdam, (1954).
- F. Mairinger and M. Schreiner, in *Science and Technology in the Service of Conservation, Preprints of IIC-Congress, Washington, 3–9 September 1982 DC*, pp. 5–15. International Institute of Conservation, London (1982).
- Materials Research Society Symposia on 'Materials Issues in Art and Archaeology,' MRS, Pittsburgh, Vols 123, Vol. 185 and 267, and Triennial Meetings of ICOM-CC (International Council of Museums Committee for Conservation), e.g. 1987 Sydney, Australia, 1980 Dresden, Germany, 1993 Washington, DC, USA, 1996 Edinburgh, UK.
- M. Marabelli and P. Santopadre (Eds), *Preprints of 2nd International Conference on Non-destructive Testing, Micro-analytical Methods and Environment Evaluation for Study and Conservation of Works of Art, Pergia 17–20.4.1988*. Instituto Centrale per il Restauro, Rome (1988).
- Ch. Wolters, in *Encyclopädie der Geisteswissenschaftlichen Arbeitsmethoden*, 6. Lieferung, p. 69. Munich (1970).
- H. Kuehn, *Maltech. Restauro* **2**, 149 (1974).
- N. S. Baer and M. J. D. Low, in *Science and Technology in the Service of Conservation, Preprints of Conservation of IIC-Congress, Washington, DC, 3–9 September 1982*, p. 1. International Institute of Conservation, London (1982).
- Ch. Lahanier, in *2nd ISCRCP, Cultural Property and Analytical Chemistry*, p. 135 (1979).
- R. Klockenkämper, A. von Bohlen, L. Moens and W. Devos, *Spectrochim. Acta, Part B* **48**, 239 (1993).
- R. Brill and S. Moll, in *Recent Advances in Conservation*, edited by G. Thomson, p. 145. Butterworth, London (1963).
- M. Schreiner and M. Grasserbauer, *Fresenius' J. Anal. Chem.* **322**, 81 (1985).
- G. Demortier, *Nucl. Instrum. Methods B* **14**, 152 (1986).
- C. Neelmeijer, W. Wagner and H.-P. Schramm, *Nucl. Instrum. Methods B* **118**, 338 (1996).
- M. A. Respaldiza and J. Gómez-Camacho (Eds), *Applications of Ion Beam Analysis Techniques and Archaeometry*. Secretariado de la Universidad de Sevilla, Seville (1997).
- W. A. Lanford, in *Handbook of Modern Ion Beam Materials Analysis*, edited by J.R. Tesmer and M. Nastasi p. 193. Materials Research Society, Pittsburgh, PA (1995).
- F. Lux, R. Zeisler and J. Reher, *Radiochem. Radioanal. Lett.* **42**, 341 (1980).
- M. Coleman and S. Walker, *Archaeometry* **21**, 107 (1979).
- H. Wulf, *Grosse Warenkunde*. Verlags ges., R. Müller, Cologne-Braunsfeld (1967).
- R. Mayer, *The Artist's Handbook of Materials and Techniques*, 5th ed. Viking Penguin, New York (1991).
- M. Mantler, *Adv. X-Ray Anal.* **41** (1999).
- R. Cesareo, G. E. Gigante, P. Canegallo, A. Castellano, J. S. Iwanczyk and A. Dabrowski, *Nucl. Instrum. Methods A* **380**, 440 (1996).
- A. Longoni, C. Fiorini, P. Leutenegger, S. Scuti, G. Fronterotta, L. Strüder and P. Lechner, *Nucl. Instrum. Methods A* **409**, 407 (1998).
- M. Mantler, M. Schreiner, F. Weber, R. Ebner and F. Mairinger, *Adv. X-Ray Anal.* **35**, 987, 1157 (1992).
- W. Neuwirth, *Loetz Austria 1900*. Selbstverlag, Vienna (1986).
- W. Neuwirth, *Loetz Austria 1905–1918*. Selbstverlag, Vienna (1986).
- J. Mergl, H. Riecke, Ch. Sellner, *Das Böhmisches Glas 1700–1950*. Passauer Glasmuseum, Passauer (1995).
- A. Burckhart, W. Stern and G. Helmig, *Keltische Münzen aus Basel*. Verlag Schweizerische Gesellschaft für Ur- und Frühgeschichte (SGUF), Basle (1994).
- R. Klockenkämper, M. Becker and H. Otto, *Spectrochim. Acta, Part B* **45**, 1043 (1990).